Motifs of the C-terminal domain of MCM9 direct localization to sites of mitomycin-C damage for RAD51 recruitment

David R. McKinzey[1] , Shivasankari Gomathinayagam[1] , Wezley C. Griffin[1] , Kathleen N. Klinzing[1] ,
Elizabeth P. Jeffries[2] , Aleksandar Rajkovic[3,4,5] , and Michael A. Trakselis[1,*]

From the [1]Department of Chemistry and Biochemistry, Baylor University, Waco, Texas, USA; [2]Department of Chemistry, University of Pittsburgh, Pittsburgh, Pennsylvania, USA; [3]Department of Pathology, [4]Department of Obstetrics, Gynecology and Reproductive Sciences, [5]Institute of Human Genetics, University of California San Francisco, San Francisco, California, USA

Edited by Patrick Sung

The MCM8/9 complex is implicated in aiding fork progression and facilitating homologous recombination (HR) in response to several DNA damage agents. MCM9 itself is an outlier within the MCM family containing a long C-terminal extension (CTE) comprising 42% of the total length, but with no known functional components and high predicted disorder. In this report, we identify and characterize two unique motifs within the primarily unstructured CTE that are required for localization of MCM8/9 to sites of mitomycin C (MMC)-induced DNA damage. First, an unconventional "bipartite-like" nuclear localization (NLS) motif consisting of two positively charged amino acid stretches separated by a long intervening sequence is required for the nuclear import of both MCM8 and MCM9. Second, a variant of the BRC motif (BRCv) similar to that found in other HR helicases is necessary for localization to sites of MMC damage. The MCM9-BRCv directly interacts with and recruits RAD51 downstream to MMC-induced damage to aid in DNA repair. Patient lymphocytes devoid of functional MCM9 and discrete MCM9 knockout cells have a significantly impaired ability to form RAD51 foci after MMC treatment. Therefore, the disordered CTE in MCM9 is functionally important in promoting MCM8/9 activity and in recruiting downstream interactors; thus, requiring full-length MCM9 for proper DNA repair.

Homologous recombination (HR) of DNA involves multifaceted processes and pathways that respond to various types of DNA damage agents encountered during S/G2 phases of mitotic cells (1, 2). Recombination occurring during meiosis can generate crossovers for genetic diversity and proper segregation in germline cells, utilizing many of the same enzymes (3, 4). Therefore, HR is vital for genomic integrity and diversity required for organismal survival. Defects in either mitotic or meiotic HR can directly contribute to increased cancer susceptibility and infertility through improper chromosomal rearrangements that represent incomplete intermediates and are hallmarks of disease. Various DNA helicases contribute to several steps in the recombination pathways either facilitating or dissolving hybrid DNA recombinants (5). Their individualized roles and substrate specificities in HR are commonly overlapping, making absolute distinctions of function difficult.

MCM8 and MCM9 are recent additions to the roster of DNA helicases involved in HR (6). They are members of the ATPases associated with a variety of cellular activities (AAA$^+$) superfamily and the minichromosome maintenance (MCM) family of proteins that includes MCM2-7 as the heterohexameric helicase complex central to the replication fork. The MCM8/9 complex does not appear to interact directly with MCM2-7, nor is it essential for replication (7). However, MCM8/9 is commonly associated with the replication fork (8) and may be able to take over helicase activities upon depletion of MCM2-7 (9), suggesting a more active and dynamic role in elongation. Mounting evidence suggests that MCM8/9 is itself a heterohexameric complex involved in mediating unknown aspects of fork progression and/or downstream HR (10–13).

Knockouts or knockdowns of MCM8 and/or MCM9 in mice and humans cause sex-specific tumorigenesis, defects in HR processing, and sensitivities to DNA damaging agents (11–15). This results in diminished DNA damage signaling as exhibited by decreased phosphorylated CHK1 (pCHK1) and increased double-strand breaks (DSBs) as indicated by H2AX foci in the presence of various fork stalling or cross-linking agents. The absence of functional MCM8 or 9 impairs HR mediated fork rescue after damage through decreased recruitment of Mre11/Rad50/Nbs1 (MRN), RPA, and RAD51. In fact, MCM8/9 has been shown to be required for MRN nuclease activity to generate single-strand DNA (ssDNA) for HR after treatment with cisplatin (Cis-Pt) (10). Even so, there are differing reports on the temporal association of MCM8/9 in relation to RAD51 after treatment with various DNA damage agents (9–12). These differences may be related to differential activities of RAD51 in HR-mediated fork stability/restart compared with that of direct DSB repair (16) from specific DNA damage agents utilized or different eukaryotic cell types.

Mutations in MCM8 and MCM9 in humans are linked to premature ovarian failure (POF) (17, 18), amenorrhea, sterility (19), and cancer (20). In fact, deficiencies in MCM8 or 9 are

---

phenotypically similar to Fanconi anemia (FA) patient mutations (21) (where ~50% of patients are infertile (22)) and suggest an overlapping role in interstrand cross-link (ICL)-coupled HR, but without the associated anemia. MCM9 mutations are also linked to hereditary mixed polyposis and colorectal cancer, commonly caused by loss of function in DNA mismatch repair (MMR) (23, 24). The MMR connection may be more important in regulating microhomology mediated HR that requires mismatch repair for Holliday junction progression (24–26) or from overlapping recognition of duplex distorting lesions (27, 28). Instead, several human cancer genomes show homo and heterozygous deletions in MCM9 coding regions, many missense mutations in MCM8 and MCM9, and altered expression levels that correlate with aggressive clinical features and poorer long-term survival in several human cancers (10, 29–31). Like that found for BRCA1/2-deficient cells, MCM8 or 9 deficient cells are hypersensitive to poly(ADP-ribose) polymerase (PARP) inhibitors indicating a link between fork progression and BRAC1/2-mediated HR repair that can be exploited in the clinic for synthetically lethal therapies with platinum-based DNA cross-linking agents (32).

MCM9 contains a unique and large C-terminal extension (CTE) not found in the other MCM family members and can be alternatively spliced to give a shorter MCM9^{M} isoform that retains the conserved helicase domains but removes the CTE (33). The CTE is a common feature in other HR helicases and is generally considered to be unstructured with scattered putative amino acid motifs that can impact protein interactions and affect proper function (6). However, no such motifs or role for the CTE has been identified for MCM9. Here, we can show that the CTE in MCM9 plays an essential role in nuclear import and formation of DNA repair foci after treatment with the cross-linking agent, mitomycin C (MMC). We have

identified and validated a unique "bipartite-like" nuclear localization signal (NLS) within the CTE that directs the nuclear import of MCM8. Finally, we have also identified a BRCv motif that is required for the recruitment of RAD51 to sites of MMC-induced damage that is analogous to that found in other HR helicases (34). The overall results confirm an influential role for the CTE of MCM9 in importing the MCM8/9 complex into the nucleus, directing it to sites of cross-link damage, and recruiting RAD51 for downstream repair.

Results

Specific domains of MCM9 reciprocally affect nuclear localization and foci formation after MMC damage

We and others have shown previously that MCM8 and MCM9 are generally localized to the nucleus and form nuclear foci after damage with MMC (11, 17). However, we sought to examine which of the domains of MCM9 (Fig. 1A) are required for nuclear foci formation after MMC treatment. MCM9 contains a unique CTE that comprises 42% of the 1143 amino acids and 52 kDa of the total 127 kDa molecular weight of the full-length protein. The CTE is more hydrophilic compared with the rest of the protein, has a higher disorder probability, and is likely mostly unstructured (Fig. S1).

As the CTE of MCM9 is predicted to have high disorder and low secondary structure, we sought to directly measure the solution structure composition of various MCM9 CTE truncations (Fig. 1B) using circular dichroism (CD). Spectra for both MCM9 643 to 900 and 680 to 900 show a pronounced minimum at 201 nm (Fig. 1C), which is consistent with significant disorder (35). There are shallow valleys from 215 to 230 nm indicative of minor α-helical and antiparallel β-sheet characteristics, but the overall spectrum is representative of a highly disordered (~50%) protein, indicated as "other" in the
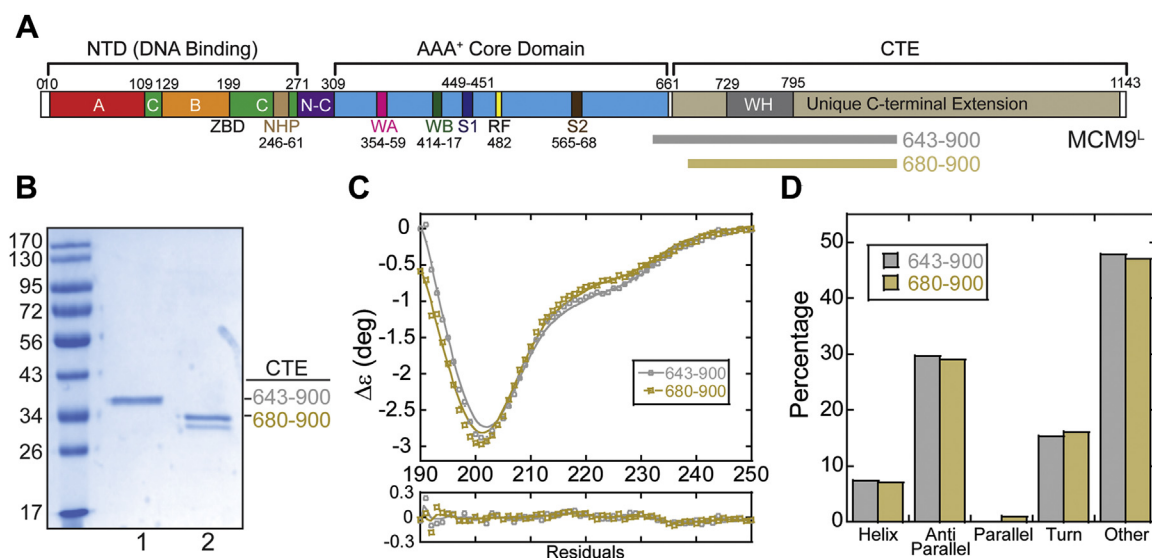

Figure 1. The CTE domain of MCM9 is largely unstructured. *A*, schematic of the full-length MCM9^{L} linear sequence identifying known domains and motifs with truncated constructs (643–900 or 680–900) indicated and shown purified on a *B*, Coomassie stained gel. *C*, circular dichroism of MCM9 C-terminal truncations, 643 to 900 (*gray*, *open circles*) or 680 to 900 (*sand*, *open boxes*), show primarily unstructured CTE truncations. Residuals of the fits (*lines*) to the data are shown below. *D*, plot of the percentage of predicted secondary structure for each truncation based on the fit of the CD data.
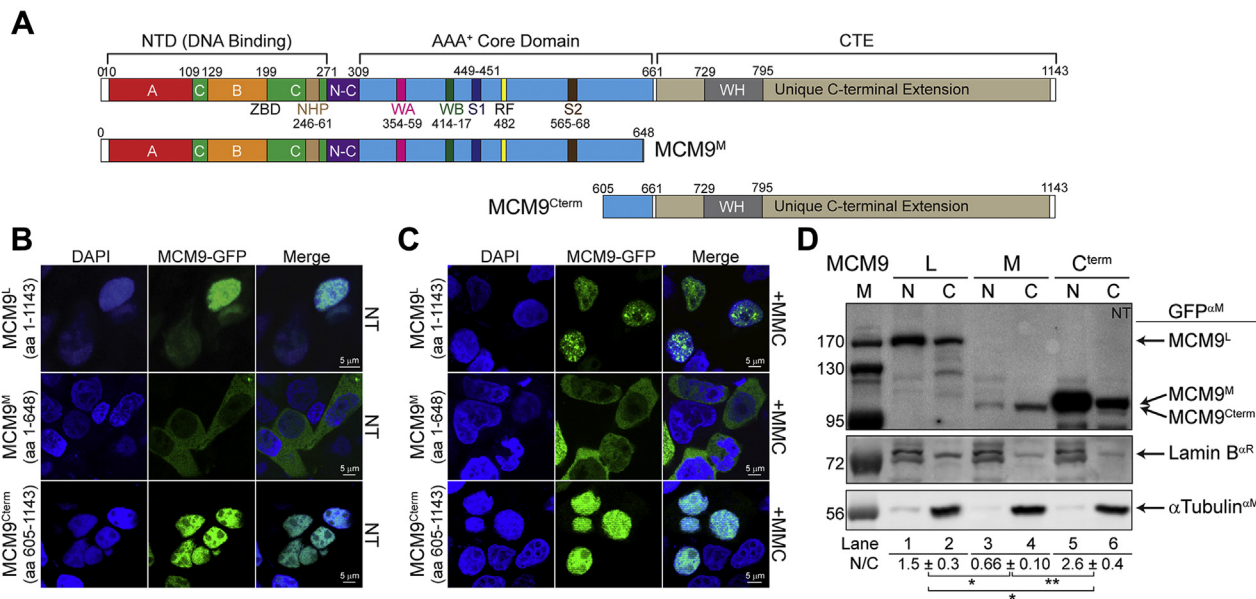
Figure 2. Full-length MCM9 forms nuclear foci with cross-link damage. *A*, schematic of the MCM9 linear sequence identifying known domains and motifs and separating MCM9^L (1–1143), MCM9^M (1–648), and MCM9^{Cterm} (605–1143). Transfection of GFP-tagged constructs in HEK293T cells either *B*, nontreated (NT) or *C*, mitomycin C (MMC) treated (3 μM). MCM9^L is nuclear and forms foci after MMC treatment, while MCM9^M is primarily cytoplasmic, and MCM9^{Cterm} is fully nuclear but without MMC-induced foci. *D*, western blot of nuclear and cytoplasmic extractions of GFP-transfected MCM9 constructs after treatment with MMC. Controls are included for nuclear (Lamin B1) and cytoplasmic (α-tubulin) fractions. Ratios of nuclear to cytoplasmic (N/C) GFP-MCM9 constructs are indicated below the image. Standard error is included for three biological replicates and the *p*-value is indicated (* <0.05; ** <0.01).

quantification (Fig. 1*D*). For the limited secondary structure, the two truncations are highly similar with only ∼7% helical and ∼30% β-sheet.

Full-length MCM9-GFP (MCM9^L) is nuclear and forms a significant number of nuclear foci upon treatment with the cross-linking agent MMC (Fig. 2, *A–C*). Interestingly, the transfection of the alternatively spliced MCM9 product (MCM9^M) (33) showed primarily cytoplasmic staining, while MCM9^{Cterm} showed concise nuclear staining but an absence of repair foci with MMC. Nuclear and cytoplasmic extractions of various MCM9-GFP transfected constructs were used to validate these observations in a population of cells and quantified by calculating nuclear/cytoplasmic (N/C) ratios (Fig. 2*D*). MCM9^L is more nuclear than cytoplasmic; MCM9^M is primarily cytoplasmic; and MCM9^{Cterm} is more nuclear, while alpha-Tubulin and Lamin B1 were used as cytoplasmic and nuclear controls, respectively. Quantification of the nuclear/cytoplasmic (N/C) ratios show values above 1 for both MCM9^L and MCM9^{Cterm} but below 1 for MCM9^M that lacks the CTE, which are statistically different. Although MCM9^{Cterm} does not form MMC-induced foci, it does interact with chromatin probably though the winged-helix domain contained in the CTE (Fig. S2). Therefore, the CTE directs MCM9 into the nucleus, but the helicase core is required for localization to DNA repair sites.

A "bipartite-like" NLS is present in the CTE of MCM9 to import MCM8/9

As MCM9^{Cterm} had predominantly nuclear staining but MCM9^M did not, we searched for nuclear localization sequences (NLS) in the CTE and found four conserved, high-confidence putative NLS sequences (pNLS) (Fig. S3). These four pNLS sequences were individually mutated in MCM9^L-GFP, transfected into U2OS cells, and the localization was examined by confocal microscopy (Fig. 3, *A* and *B*). U2OS cells were used because of their larger nuclei that can be easily distinguished from cytoplasmic areas. Mutation of pNLS1 or pNLS2 resulted in primarily cytoplasmic staining indicating a lack of nuclear import. Alternatively, mutation of pNLS3 and pNLS4 had no noticeable effect on nuclear import. Interestingly, mutation of either pNLS1 or pNLS2 alone had a clear effect on nuclear import, indicating that a bipartite NLS1/NLS2 is required; however, the linker between NLS1 and NLS2 spans 67 a.a., much longer than a canonical bipartite NLS that generally has a 10 to 12 a.a. linker. Therefore, the import signal motif for MCM9 is "bipartite-like" consisting of dual NLS1/NLS2 motifs connected by an extended linker region.

To unequivocally show the effect of mutating NLS1 or NLS2 in a population of cells, we performed nuclear and cytosolic extractions on MCM9^L-GFP construct transfected into 293T cells (Fig. 3*C*). Again, wild-type (WT) MCM9^L is confined more in the nuclear fraction than the cytoplasm as indicated by N/C = 1.5. However, mutation of either NLS1 or NLS2 shows a significant decrease in the N/C ratio. This result confirms a requirement for both NLS1 and NLS2 in the CTE of MCM9 for efficient import into the nucleus.

We also searched *in silico* for a pNLS in MCM8, but no high-confidence motifs were detected. Therefore, we hypothesized that the NLS1/2 in the CTE of MCM9 may be responsible for nuclear import of the MCM8/9 complex. Therefore, we created custom CRISPR-Cas9 MCM8 or MCM9
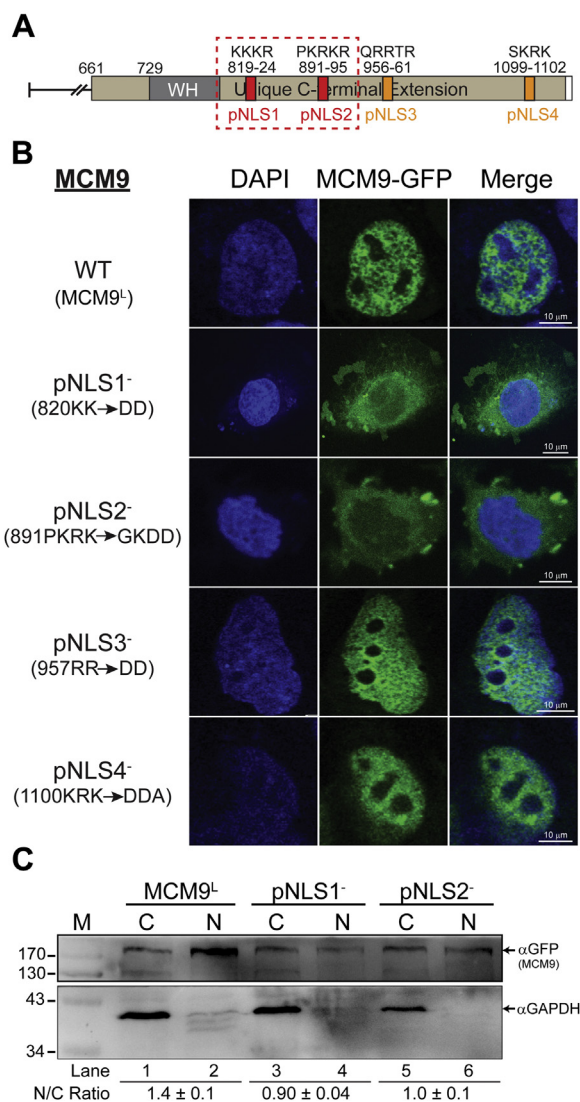
Figure 3. A "bipartite-like" NLS1/2 is required for nuclear localization. *A*, four putative nuclear localization sequences (NLS) were identified *in silico*. *B*, mutation of these NLS sequences in GFP-MCM9^L was tested for any effect on location to the nucleus in U2OS cells. *C*, nuclear and cytoplasmic extractions of GFP-transfected MCM9 constructs. GAPDH is used as a control for cytoplasmic proteins. Ratios of nuclear to cytoplasmic (N/C) are indicated below the image. M is for molecular weight markers indicated on the left of the blot.

Figure 4. MCM9 is required for nuclear import of MCM8. MCM8-GFP was transfected into *A*, 293T or *B*, 293T-MCM9^{KO} cells in either nontreated (NT) cells or cells treated with 3 μM MMC. *C*, conversely, MCM9^L or MCM9^M-GFP was transfected into MCM8^{KO} cells.

knockout cell lines from 293T cells with significant multiallelic indels and validated phenotypically with severe MMC sensitivity (Fig. S4). To confirm if knockout of MCM9 disrupts import of MCM8 into the nucleus, MCM8-GFP was transfected into the MCM9^{KO} cell line (Fig. 4*B*). In WT 293T cells, MCM8-GFP is primarily nuclear and forms foci with MMC treatment (Fig.4*A*); however, in MCM9^{KO} cells, the MCM8-GFP staining is diffuse throughout the cytoplasm, not localized to the nucleus, and fails to form MMC-induced nuclear foci (Fig. 4*B*). Transfection of MCM9^L-GFP or MCM9^M-GPF into MCM8^{KO} cells (Fig. 4*C*) shows essentially the same results (as in Fig. 2, *B* and *C*) with nuclear and cytoplasmic staining, respectively. Therefore, MCM8 is imported into the nucleus complexed with MCM9 as directed by the "bipartite-like" NLS1/NLS2.
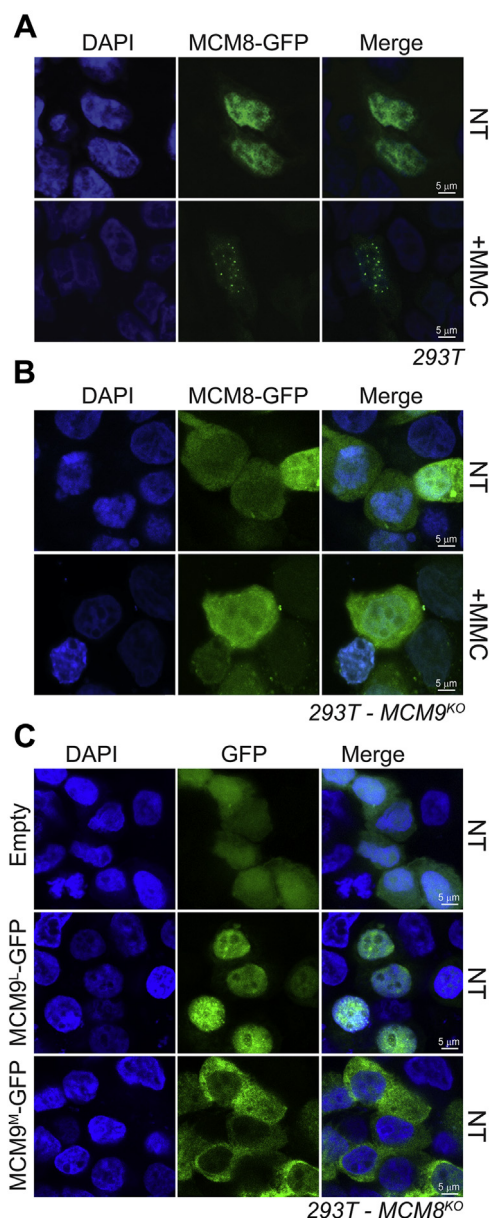
A BRCv motif is present in the CTE of MCM9

The BRC repeat sequence is a structural motif in the breast cancer type 2 susceptibility protein (BRCA2) that is utilized to promote RAD51 nucleoprotein filament formation during fork reversal or recombination (36). The eight repeats in BRCA2 show a consensus BRC motif sequence (Fig. S5), and variants of these BRC motifs (BRCv) have been found in other proteins including RECQL5 and yeast helicases Srs2, Sgs1, Mph1, and Pif1 (34). The BRCv motif in RECQL5 is shown to be important for interacting with RAD51, directing D-loop and filament formation, and responding to cross-linking stress.

In our examination of the expansive and unique CTE of MCM9, we also identified a putative BRCv motif that is similar to that found in RECQL5 and adjacent to a predicted WH
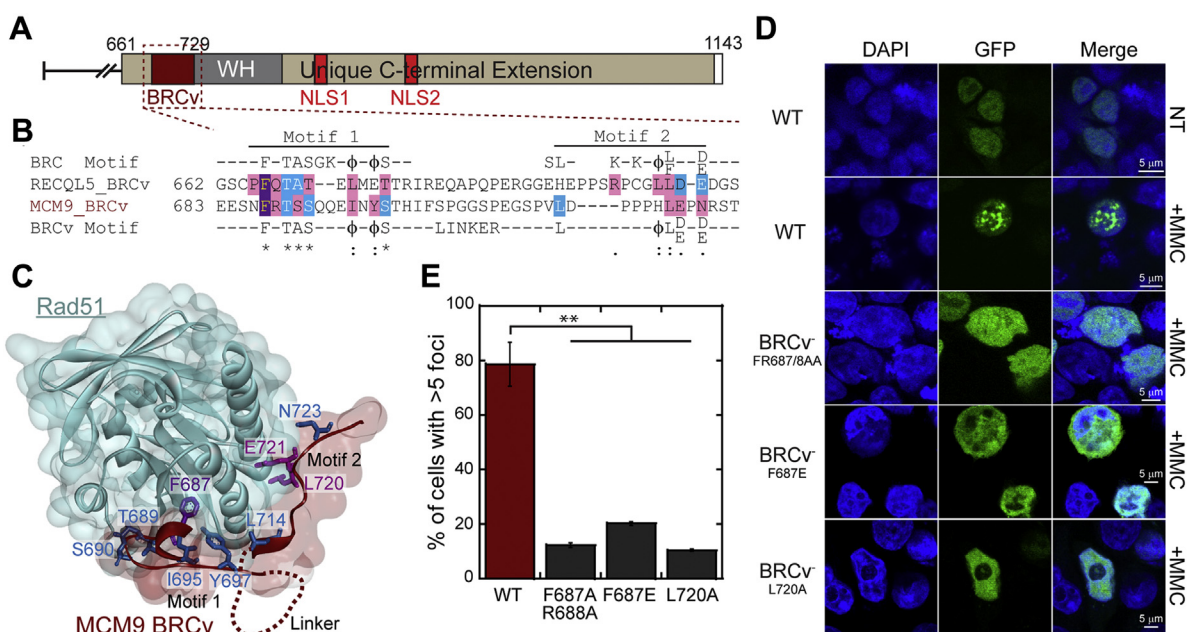
Figure 5. A BRCv motif in MCM9 is required for foci formation with MMC. *A*, a BRCv motif was identified in the CTE of MCM9 and *B*, aligned with the BRC consensus sequence and a previously identified BRCv motif in RecQL5. *C*, the MCM9 BRCv peptide was homology modeled onto the structure of RecQL5 BRCv with Rad51 (PDBID:1N0W) visualizing the impact of conserved residues. *D*, GFP-MCM9^L(BRCv-) constructs (FR687/8AA and F687E targeting Motif 1 and L720A targeting Motif 2 were transfected into HEK293T cells and *E*, show significantly reduced nuclear foci after MMC (3 μM) treatment (**p-value < 0.01). Error bars are standard error of three biological replicate experiments.

motif important for DNA binding (Fig. 5, *A* and *B*). The BRCv consensus sequence within motif 1, FxTASxxxΦxΦS, is highly similar to the BRC repeats themselves FxTASGKxΦxΦS (where "Φ" represents hydrophobic residues). BRCv motif 2 occurs after a linker region in these HR helicases that is not present in BRCA2 and is less well conserved. However, a small hydrophobic/electrostatic patch in Motif 2, ΦL(D/E)-(D/E), is present in MCM9 and similar to RECQL5. Both BRCv motifs 1 and 2 in MCM9 are well conserved across Mammalia species, but less conserved in other metazoans (Fig. S5*B*).

Structural modeling of the MCM9 BRCv motif threaded onto BRCA2-BRC4 component in complex with RAD51 (34) shows the importance of the universally conserved F687 residue binding deep into a hydrophobic pocket of RAD51 (Fig. 5*C* and Fig. S5*C*). Other conserved residues (T689, S690, S691, I695, and Y697) within motif 1 make backbone and side-chain contacts across a path of hydrophobic surface area. Residues within motif 2 make both hydrophobic and hydrogen bonding contacts with RAD51 that would loop out the linker region in between (Fig. S5, *D* and *E*). Leu714 is predicted to make hydrophobic contacts with RAD51 residues 254-5 and 258-9. Our model also predicts that Glu722 and Asn724 make H-bond contacts with Tyr205 and Arg250 of RAD51, respectively. Together MCM9 BRCv motifs 1 and 2 are predicted to make sufficient hydrophobic surface area contacts with RAD51 that are anchored by F687.

To test whether mutation of the MCM9 BRCv motif has any effect on foci formation in MMC treated cells, we transfected mutated MCM9-GFP constructs (FR687/8AA, F687E, and L720A) into 293T cells (Fig. 5, *D* and *E*). The GFP fluorescence for the BRCv mutants was nuclear as expected, but MMC did not induce significant foci formation in any of these mutants. Quantification of cells with >5 foci with MMC treatment for WT (78.7 ± 8.0%) *versus* BRCv⁻ mutants: F687A/R688A (12.2 ± 0.8%), F687E (20.2 ± 0.8%), and L687A (10.4 ± 0.5%) show significant differences (Fig. 5*E*) and illustrate the importance of the bipartite BRCv motif in directing downstream DNA repair.

MCM9 recruitment is upstream of RAD51 during MMC treatment

As both BRCA1 and RAD51 form MMC-induced nuclear foci (37) similar to MCM9, we sought to examine whether there is colocalization of these two known ICL/HR proteins with MCM9 after DNA damage. BRCA1 has dual and independent functions in ICL repair and HR (38) but importantly acts upstream of RAD51. BRCA1 interacts with FANCI/D2 complex in the Fanconi cross-link repair pathway and works to stabilize stalled/reversed forks to facilitate ICL repair (39–41). Previously, it was shown that the MCM8/9 complex is rapidly recruited to direct DSBs caused by *I-SceI* and promotes the association of RAD51 directly with MCM9 for HR (9, 12). However, an earlier report suggested that MCM8/9 acted downstream of RAD51 in DT40 cells treated with MMC or Cis-Pt (11), suggesting possible differences in cell types and ICL *versus* HR repair.

Using the cross-linking agent MMC, both BRCA1 and MCM9 nuclear foci are increased in 293T cells as expected (Fig. 6*A*). Furthermore, BRCA1 foci appear colocalized with MCM9 foci. MMC-induced MCM9 nuclear foci also colocalize with RAD51; however, this is incomplete as individual RAD51 foci are apparent without MCM9 (Fig. 6*B*).
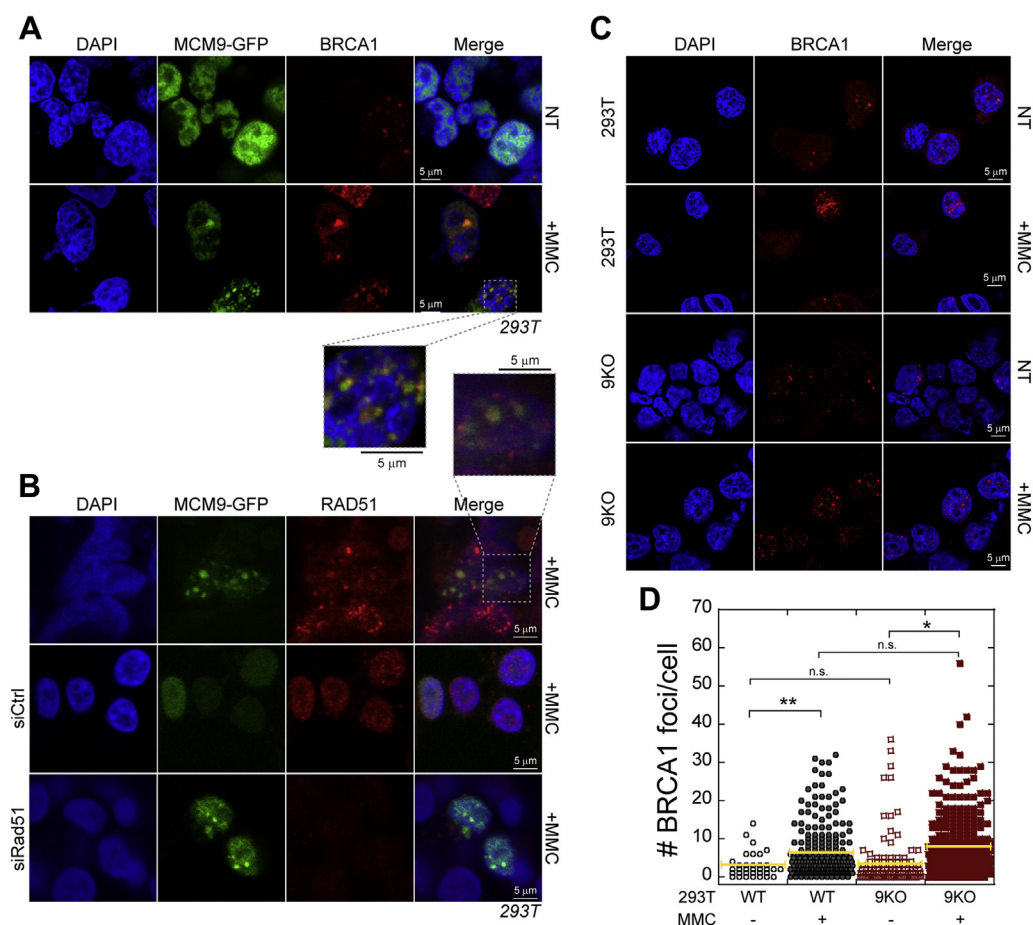
Figure 6. MCM9 colocalizes with other HR proteins and acts upstream of RAD51. *A,* MCM9 colocalizes with BRCA1 and partially colocalizes with *B,* RAD51 in MMC (3 μM) treated HEK293T cells. Knockdown of Rad51 by siRNA has no effect on MMC-induced MCM9 foci formation. *C,* BRCA1 foci per cell in nontreated (NT) and MMC treated 293T or MCM9[KO] (9KO) cells were *D,* quantified for more than 150 cells for each condition and include two biological replicates. *Yellow bar* represents the average (**p < 0.01; *p < 0.05; n.s., not significant).

Interestingly, siRNA knockdown of RAD51 significantly reduced the RAD51 foci formation but left MCM9 foci intact (Fig. 6*B* and Fig. S6). This suggests that MCM9 is acting upstream and is required (either directly or indirectly) for the recruitment of RAD51 in the MMC-induced DNA repair pathway.

To test the dependance of MCM9 in the temporal recruitment of other known effectors in the cross-link-HR pathway, we tested the ability of BRCA1 to form MMC-induced foci in MCM9[KO] cells. In 293T cells, there is a significant increase in the number of BRCA1 foci per cell when treated with MMC (2.9 ± 0.6 *versus* 6.2 ± 0.5) as expected (Fig. 6, *C* and *D*). A similar increase in BRCA1 foci is observed in MCM9[KO] cells when treated with MMC (3.4 ± 0.6 *versus* 7.8 ± 0.4) (Fig. 6, *C* and *D*). Although there is a slight increase in BRCA1 foci in MCM9[KO] *versus* WT cells, this is not significant in our analysis. Therefore, the BRCA1 response to MMC treatment is not dependent and appears generally unaffected by the absence of MCM9.

As we had previously characterized MCM8 and MCM9 mutations of POF patients within consanguineous families, we examined whether these conditioned mutations in MCM9 impaired RAD51 foci formation with MMC treatment (Fig. 7,

A and *B* and Fig. S7). 8AIV-3 designates patient EBV transformed lymphocytes from an affected MCM8 family (17) but is fully WT for both MCM8 and MCM9, acts as a suitable control, and shows significant RAD51 foci after MMC damage as expected. 9BII-4 designates lymphocytes from a heterozygous family member with one WT allele and one splice site mutation that eliminates the CTE of MCM9 (18). Even in these WT/MT cells, RAD51 foci formation is impaired and diffuses throughout the nucleus suggesting that MCM9 copy number and the CTE are important in promoting downstream repair by RAD51. Finally, 9AII-6 designates lymphocytes from a fully homozygous (MT/MT) affected patient where a nonsense mutation in exon 2 effectively creates a complete knockout of MCM9 (18). In 9AII-6 cells, there is also a complete lack of RAD51 foci and diffuse nuclear staining with MMC-induced damage.

To confirm this dependency of MMC-induced RAD51 foci on MCM9, we changed the experiment to quantify RAD51 foci in 293T WT cells *versus* their MCM9[KO] counterparts. Treatment of 293T WT cells with MMC showed a significant increase in the number of foci per cell (6.1 ± 0.5 *versus* 21.2 ± 0.8), as expected (Fig. 7, *C* and *D*). Conversely, RAD51 foci in MCM9[KO] cells were not significantly increased with MMC
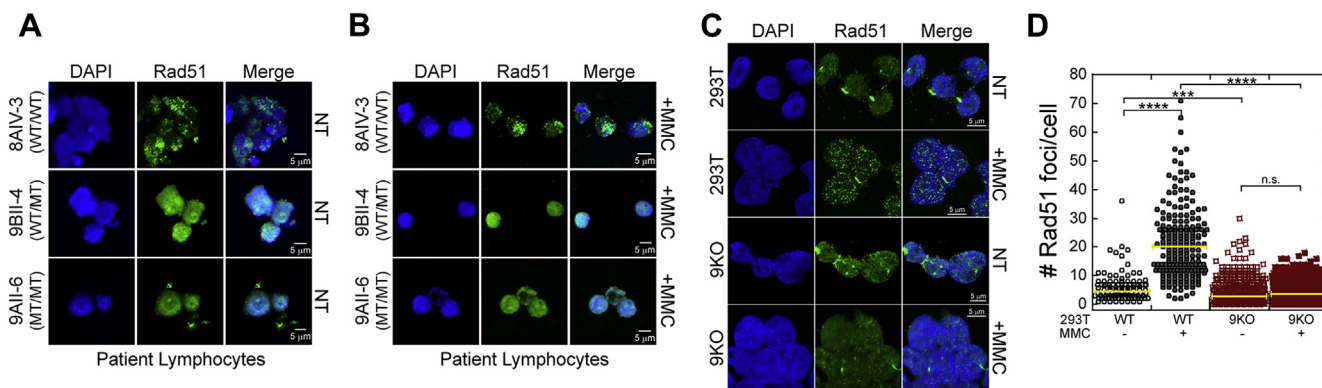
Figure 7. MCM9 is required for recruitment of RAD51. Rad51 localization in *A*, nontreated (NT) and *B*, foci formation after MMC (3 μM) treatment are disrupted in MCM9-deficient patient EBV-transformed lymphocyte cells. 8AIV-3 is wild type for both MCM8 and MCM9. 9BII-4 is heterozygous for a splice site mutation effectively eliminating the C-terminal half of MCM9. 9AII-6 is homozygous affected by a nonsense mutation in exon 2 that effectively creates a complete knockout of MCM9. *C*, MMC-induced Rad51 foci are also *D*, significantly reduced in MCM9^{KO} (9KO) cells and not significantly increased with MMC treatment. Foci per cell were quantified for more than 200 cells for each condition for two biological replicates. *Bar* represents the average (****$p < 0.0001$; ***$p < 0.001$; n.s., not significant).

treatment (4.4 ± 0.2 *versus* 4.8 ± 0.2). Interestingly, the number of RAD51 foci were also significantly decreased in MCM9^{KO} cells compared with WT cells. Collectively, these data support the conclusion that RAD51 recruitment and loading for downstream repair of MMC-induced DNA damage are likely dependent on an interaction with the BRCv motif in MCM9.

RAD51 physically interacts with the BRCv of MCM9

In order to test whether the BRCv within the CTE of MCM9 is utilized for the direct interaction with RAD51, we switched to more explicit biochemical assays including a GST pull-down (Fig. 8*A*). A GST-RAD51 construct was expressed, purified, and bound to GST resin before the addition of the CTE of MCM9 (643–900 a.a.). Some MCM9 flowed through indicating either overloading or more likely a weaker interaction, but after seven washes, even more MCM9 was eluted after addition of glutathione. Further constructs of different lengths and truncations containing the BRCv mutation were prone to aggregation and insolubility issues with lower purification yields.

Therefore, we switched to a yeast two-hybrid (Y2H) assay to test the effect of a BRCv mutation on the interaction with RAD51 (Fig. 8, *B–D*). Both positive (1) and negative (2, 7–10) controls grew and behaved as expected in a filter-based β-galactosidase assay: blue—positive, white—negative. Both full-length MCM9 (3) and the CTE only (4) showed blue color indicative of an interaction with RAD51. Mutation of the BRCv motif in both constructs (5, 6) eliminated the positive blue color consistent with a disruption of the RAD51 interaction.

Discussion

The CTE domain of MCM9 is long and primarily unstructured; however, we identified two amino acid motifs that are necessary for both the nuclear import of the MCM8/9 complex and their response to cross-link damage (Fig. 9). The NLS motif is "bipartite-like" consisting of two positively charged amino acid stretches separated by a longer unstructured and unconventional 67 amino acid linker. The BRCv motif is also bipartite, utilized for localization to sites of MMC-induced DNA damage, and promotes the association of RAD51 for downstream repair. Interestingly, MCM9 appears to be present at the replication fork (8) and can likely respond early to MMC-induced damage by recruiting RAD51 for recombinational repair.

Unstructured C-terminal tails are common in DNA repair proteins

The CTE of MCM9 is translated primarily from the last exon (exon 12) and appears to be a later evolutionary addition to the MCM9 gene (33). MCM9 is almost universally present together with MCM8 and is distributed in most opisthokonts, excavates, and chromalveolates (42). Interestingly, MCM9 is fully present in plantae; however, the terminal exon giving rise to the CTE is absent in this eukaryotic supergroup. MCM9 members are absent in some opisthokonts, which include animals and fungi, but of those present, the primary isoform includes the CTE, while other isoforms are alternatively spliced for shorter proteins.

Several DNA replication and repair proteins contain large unstructured regions or domains that are required for proper function including several translesion synthesis DNA polymerases (43, 44), DNA replication initiation proteins (45), various DNA repair helicases (6), mismatch repair proteins (MutLα) (46), nucleotide excision repair proteins (XPA) (47), the heterotrimeric single-stranded binding protein (RPA) (48), and even the tumor suppressor p53 (49). Some residues in these regions are posttranslationally modified, but there are also specific motifs that are either structured on their own or adopt structure in order to control their localization, interactions, and/or functions. Previously, a role for the CTE of MCM9 was unknown. No posttranslational modifications are known to occur in the CTE, but we have validated both an unconventional bipartite-like NLS and a bipartite BRCv motif that are required to direct function of MCM8/9 to facilitate MMC-induced DNA damage repair.
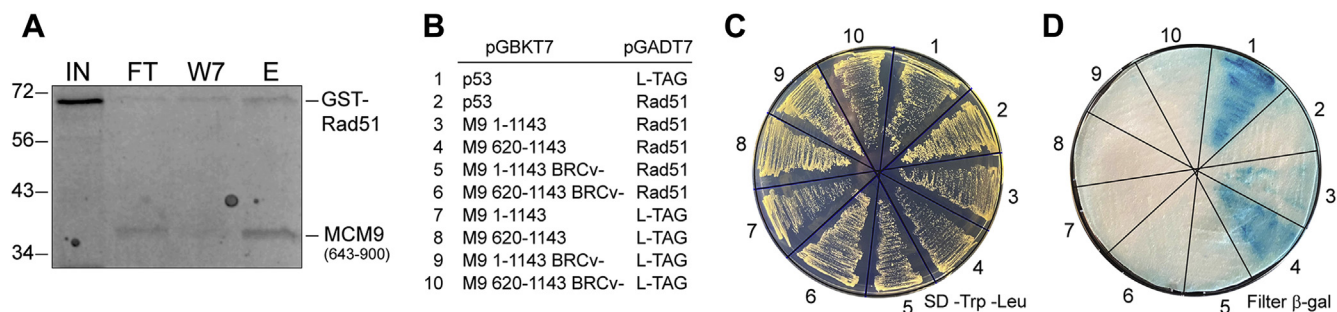
Figure 8. RAD51 interacts directly with the BRCv domain of MCM9. *A,* pull-down of MCM9 (643–900) is present with GST-RAD51 immobilized to GST-agarose and eluted with glutathione after seven washes. Molecular weight markers (kDa) are indicated on the *left* of the gel. *B,* yeast two-hybrid analysis (strain: SFY526) plated on *C,* SD–TRP/-LEU and then *D,* transferred to a filter-based X-gal assay. RAD51 and MCM9 interactions confirmed through the BRCv motif of MCM9. BRCv⁻ mutation is F687A/R688A. E, elution; FT, flow through of MCM9 (643–900); IN, input GST-RAD51; W7, seventh wash.
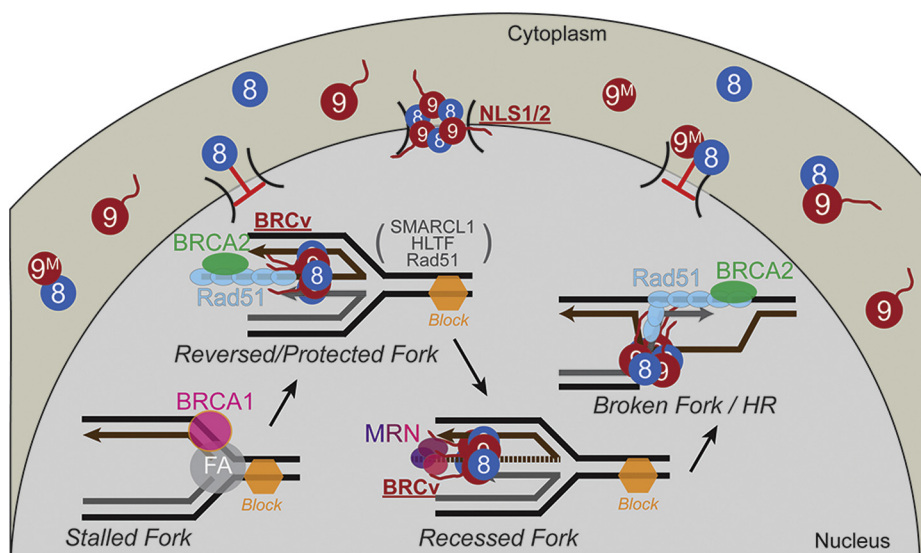

Figure 9. Model for MCM8/9 recruitment of RAD51 to sites of damage. The C-terminal bipartite-like NLS1/2 motif in MCM9 is responsible for nuclear import of MCM8/9, and the BRCv motif is required for recruiting and loading of RAD51 to sites of MMC-induced DNA damaged forks.

MCM9 has an unconventional "bipartite-like" NLS

Classic NLS (cNLS) motifs are generally recognized as clusters of basic amino acids that are either monopartite or bipartite (50, 51). Bipartite NLS motifs are conventionally described as being separated by 10 to 12 residues based on the initial characterization of the cNLS of *Xenopus laveis* nucleoplasmin (52). However, other bipartite cNLS with longer or extended linkers (20–25 residues) has been characterized in Smad4 (53), *Aspergillus* topoisomerase II (54), and XRCC1 (55, 56), and systematic extension of the linkers in bipartite cNLS has shown that longer linkers can be utilized in nuclear import (57, 58). Yet, the linker region between NLS1 and NLS2 of MCM9 is 67 amino acids and is to our knowledge one of the longest, prompting us to term this "bipartite-like" NLS1/2.

Nuclear import of a bipartite NLS involves the binding of the upstream and downstream basic residues to minor and major binding pockets, respectively, for importin-α (59, 60). Both backbone and side-chain interactions can be made from the linker region to a region between binding pockets. Once bound, Importin-α transports the cargo protein along with Importin-β through the nuclear pore complex depositing into the nucleus (61). It is hard to imagine that the longer un-structured linker between NLS1 and NLS2 in MCM9 would make specific contacts in this region, although this remains to be determined. However, we would predict that both NLS1 and NLS2 are required to bind to the binding pockets of Importin-α to facilitate import.

Based on our results, the "bipartite-like" NLS1/2 in MCM9 is also responsible for the nuclear import of MCM8. MCM8 is presumed to be constitutively bound to MCM9 after translation to form a higher-order oligomeric complex. MCM8 is devoid of any identifiable NLS and, based on its large molecular weight, would require an association with a partner for nuclear import. This is reminiscent of DNA ligase 3 (Lig3α) being bound to XRCC1 for cotransport into the nucleus for DNA repair (62). Another example includes the bipartite NLS in Smad4 being utilized for import of other complexed and phosphorylated Smad proteins for transcriptional regulation (53). Interestingly, several studies have shown that knockdown or knockout of MCM8 also eliminates MCM9, but that

knockdown of MCM9 has more of a singular effect (12, 14). Therefore, we would hypothesize that MCM9 is stabilized by the presence of MCM8 in an MCM8/9 complex and MCM8, although stable on its own, is unable to be imported into the nucleus. This would represent an important regulatory mechanism for ensuring that MCM8/9 is in a complex and not represented as individual components.

MCM9 has a BRCv motif in the CTE

The BRC repeats are hallmarks within the BRCA2 protein required for interactions with RAD51 during HR and are not typically found in other proteins. A variant BRC motif (BRCv) has been characterized in the human DNA repair helicase, RECQL5, and other BRCv motifs are predicted to be present in other DNA repair helicases including yeast Srs2, Mph1, Sgs1, and Pif1 (34). The BRCv in MCM9 shows high homology to the motifs 1 [FXTA(S/T)] and 2 [Φ(L/F)XX(D/E)] in RECQL5 with an equivalent 14 amino acid linker region between both motifs. Like that for RECQL5, BRCv motif 1 appears to be more conserved and makes more intimate contacts with the oligomerization interface of RAD51. Besides the conserved F687 and residues adjacent, I695 in MCM9 is homologous with L672 in RECQL5 as a small hydrophobic residue that is important for RAD51 association (34). When modeled for MCM9, L672 makes significant contacts in the hydrophobic patch adjacent to F687 making up a lynchpin for binding. Motif 2 is just adjacent to the proposed binding site for motif 1 and acts to strengthen bipartite binding to RAD51 through conserved central hydrophobic residues that include L720. Interestingly, the linker region is not conserved between these helicases and would represent an extruded unstructured area only required as a spacer for proper positioning of motif 2. Therefore, like RECQL5, our data support the conclusion that the BRCv motif in MCM9 is required to regulate RAD51 recruitment and filament formation to mediate fork restart or recombination activities at the replication fork during times of stress.

MCM9 aids in the recruitment of RAD51 to MMC-induced sites of damage

There appears to be two conflicting viewpoints for when MCM8/9 temporally responds to various types of DNA damage in relation to RAD51. Several lines of evidence examining the cellular role of MCM8/9 come primarily from responses to the cross-linking agent (Cis-Pt) and correlate to a purported activity in later stages of HR downstream of RAD51 synapsis (9, 11). In those studies, RAD51 foci formed after Cis-Pt treatment are still present in MCM8 or 9 knockout cells, indicating no dependence of RAD51 on MCM8/9. This directly contradicts work here, which shows severely decreased RAD51 foci in patient deficient MCM9 cells after treatment with MMC, indicating a codependence for MCM8/9 with RAD51. Instead, these results correlate with MCM8/9 acting upstream of RAD51 after treatment with MMC, consistent with other studies in human/*Xenopus* systems (10, 12). MCM8/9 are present early in the ICL/HR repair pathway during fork stalling, reversal, stabilization, and prior to RPA binding or synapsis (10, 12, 14) but are not dependent on BRCA1. MCM8/9 also colocalize with BRCA1 and a subset RAD51 foci in humans; however, MCM8/9 are required for RAD51 foci formation but not for that of BRCA1. To reconcile these discrepancies, it is probable that MCM8/9 are responding to yet unknown specificities and overlapping aspects of DNA recombination associated with fork stalling, ICLs, and DSBs dependent on RAD51 that will require further experimental depth.

Cross-linking agents such as Cis-Pt and MMC are commonly thought of in the same vein, and although both typically only cause about 5 to 10% ICLs, they have different targets and effects on duplex structure (63, 64), which may be responsible for different temporal recruitment of MCM8/9. Cis-Pt cross-linking occurs at N7 of guanine at either 5'-GpG or 5'-ApG resulting primarily in intrastrand cross-links and <8% ICLs (65). MMC reacts with the N^2 exocyclic amine of guanine preferentially at 5'-CpG sites forming monoadducts that insert into the minor groove and can form ICLs across in about 10% of products (64, 66, 67). However, the major difference between Cis-Pt and MMC is their effects on duplex structure. Cis-Pt induces major helical distortion with both monoadducts and ICLs underwinding the helix, bending of the strands inward, and flipping out of the unpaired cytosines (68). On the other hand, MMC causes minimal distortion, no bending, and maintains the C-G base pairs even with the G-mito-G ICL (69). These differences will be important in understanding MCM8/9 specificities, recruitment, and effects on RAD51 pathways moving forward.

Single monoadducts or intrastrand cross-links on either the leading or lagging strands are blocks to DNA synthesis decoupling the replisome, while ICLs are total replisome blocking adducts. In these scenarios, various mechanisms of recombination would be utilized including fork reversal, template switching, and single-strand breaks repaired by sister chromatin recombination. It is probable that Cis-Pt and MMC direct MCM8/9 to act differentially in recruiting RAD51 in multiple pathways for repair. Damage from Cis-Pt is primarily recognized and repaired by nucleotide excision repair (NER) (70, 71), but because the duplex is distorted, the mismatch repair (MMR) pathway also contributes (72, 73). On the other hand, MMC lesions may only be recognized during active DNA replication processes and repaired by various translesion synthesis (TLS), HR, and NER pathways (74).

Therefore, our work here has provided evidence that the CTE within MCM9 is important in regulating MCM8/9 activities at sites of DNA damage. Entry into the nucleus after translation is directed through an unconventional "bipartite-like" NLS in the CTE of MCM9 that imports MCM8/9 as a complex. Once there, MCM8/9 associates with the replisome to actively respond to DNA damage encountered during synthesis. Recruitment of RAD51 occurs through a bipartite BRCv motif in the CTE of MCM9 that carries out downstream recombination. Even so, further efforts are needed to

better understand the specific enzymatic functions and interactions of MCM8/9 in relation to different DNA damage agents to more specifically describe its reported helicase function in relation to the many other analogous HR helicases.

Experimental procedures

Materials

Oligonucleotides were purchased from Sigma or IDT. ON-TARGET *plus* siRNA to RAD51 from Dharmacon. Mission siRNA and universal negative control #1 was from Sigma-Aldric. Mitomycin C (MMC) was from Thermo Fisher. Restriction enzymes from New England Biolabs. All other chemicals were analytical grade or better.

Cloning

pEGFPC2-MCM9 full length has been described previously (18). The truncated mutants—MCM9^{Cterm} (a.a. 605–1143), MCM9^{M} (a.a. 1–648) were created by traditional restriction site cloning into pEGFP-C2 using *XhoI*/*XmaI*. Codon-optimized MCM9 for bacterial expression (a.a. 643–900 or 680–900) (Genewiz) were cloned into pGEX-6P1 using *BamHI* and *XhoI* restriction sites. Mutants at putative nuclear localization sites: pNLS1 (820KK→DD), NLS2 (891PKRK→GKDD), NLS3 (957KK→DD), NLS4 (1099KRK→DDA), and BRCv (687FR→AA, 687F→E, or 720L→A) sites were created by QuikChange mutagenesis (Agilent Genomics) using Kapa DNA polymerase (Kapa Biosystems) and screened with novel silent restriction sites. All primers are listed in Table S1. All mutations were confirmed at the Genomic Sequencing and Analysis Facility (University of Texas Austin).

Sequence analysis, alignments, and protein homology modeling

The amino acid sequence of human MCM9 (Accession: NP_060166.2) was analyzed using ProtScale (https://web.expasy.org/protscale/) according to the Kyte and Doolittle model of hydropathicity (75). The disorder probability was calculated using DISOPRED (http://bioinf.cs.ucl.ac.uk/disopred/) (76). The secondary structure prediction was calculated using PSIPRED 4.0 (http://bioinf.cs.ucl.ac.uk/psipred/) (77). The four highest-confidence NLS sites for MCM9 were predicted and determined by NLS Mapper (http://nls-mapper.iab.keio.ac.jp) (78). The BRCA2 BRC4-RAD51 crystal structure (PDBID: 1N0W) was used to create a homology model for the BRCv motif of MCM9 (a.a. 682–700, 713–726) using Swiss-Model server (https://swissmodel.expasy.org/) (79) and validated using QMEAN (https://swissmodel.expasy.org/qmean/) (80).

Protein purifications

GST-tagged RAD51 was purified as described previously (81). C-terminally truncated MCM9 constructs (643–900 or 680–900) with GST at the N-terminus were transformed into C43 pLysS (Lucigen) and induced with 0.25 mM IPTG at OD$_{600}$ ∼ 0.5 for 4 h at 37 °C. Pellets were resuspended in lysis buffer (20 mM HEPES pH 8.0, 300 mM NaCl, 10 mM BME, 10 mg/ml lysozyme, 0.1% Triton-X 100, 1 mM PMSF, 1 mM EDTA, 4 μg/μl pepstatin A) on ice. The clarified lysate was loaded onto the GSTrap column in Buffer A (20 mM HEPES pH 8.0, 300 mM NaCl, 10 mM BME, 1 mM EDTA, 10% glycerol) and eluted with Buffer B (Buffer A + 10 mM gluta-thione). Fractions were concentrated using a spin concentrator and rocked overnight at 4 °C with TEV protease. The cleaved product was applied again to a GSTrap column, and the flow through collected. Purity was confirmed to be greater than 95% by SDS-PAGE, and the concentration was determined by absorbance using ε = 12,615 M^{-1} cm^{-1}.

Circular dichroism

CD spectra of 5 μM purified MCM9 643 to 900 and 680 to 900 were collected using a Jasco J-815 spectropolarimeter at room temperature (23 °C) in 10 mM potassium phosphate buffer (pH 7.0) containing 100 mM (NH$_4$)$_2$SO$_4$ using a 0.1 cm quartz cell. Five individual spectra were collected using a 1 nm bandwidth at 0.5 nm intervals at a speed of 50 nm/min before averaging. The raw data in measured ellipticity (ε) was then analyzed using BeStSel (http://bestsel.elte.hu/index.php) for conversion to Δε units and determination of secondary structure (82, 83). All data points analyzed were collected under a HT measurement of 800 V. Secondary structure predictions had NRMSD values <0.05.

Cell culture

HEK293T or U2OS cells were grown in Dulbecco's modified Eagle's medium (DMEM) (Corning Cellgro) with 10% fetal bovine serum (FBS) (Atlanta Biologicals) and 1% penicillin/streptomycin (P/S) (Gibco) in 5% CO$_2$ at 37 °C. Patient EBV transfected lymphocytes (17, 18) were grown in suspension in RPMI 1640 (Corning) with 10% FBS and 1% P/S.

Cell transfection and treatment

HEK293T or U2OS cells plated on poly-lysine-coated coverslips were transfected with the respective EGFP-MCM9 constructs using linear polyethyleneimine (LPEI) or lipofectamine 3000 (Thermo Fisher) according to manufacturer's directions. Briefly, transfection reagent and plasmids were incubated at RT for 10 min and added to cells in Opti-MEM serum-free media (ThermoFisher) or DMEM 10% FBS with no antibiotics. siRNA RAD51 knockdown or the universal negative control #1 was transfected alone or in combination with a plasmid using Dharmafect1 or DharmafectDuo (Dharmacon). The transfection mixture was removed after 6 h and replaced with DMEM/10% FCS for up to 24 h. The cells were then treated with indicated concentrations of MMC (Sigma-Aldrich) for 6 h. Posttreatment, the cells were immediately prepped for western blotting, direct confocal microscopy, or immunofluorescence. Western blots were probed with RAD51 (H-92 or sc-8349) and α-tubulin (TU-02) antibodies (Santa Cruz Biotechnology Inc). Fluorescent secondary antibodies were α-rabbit IgG-Alexa488 or α-mouse IgG-Alexa647

conjugates (ThermoFisher). Membranes were scanned using the LAS 4000 imager (Cytiva).

CRISPR-Cas9 gene knockouts

Guide RNAs were designed using CRISPR design tool (Perkin Elmer-Horizon) targeting MCM8 and MCM9. The following target sequences were used: ATGTTGACTG CATTGACTGT GGG (MCM8) and AGCGATCAAGTTA CACTGGTTGG (MCM9). Targeting sequences were cloned into pSpCas9(BB)-2A-Puro (PX459) V2.0 (Addgene #62988) using *BbsI*. HEK293T were transfected with either the plasmid containing the gRNA sequence for MCM8 or MCM9 or empty vector. After transfection, cells were incubated for 48 h in DMEM 10% FCS and then split into DMEM 10% FCS containing 1 µg/ml puromycin (Thermo Fisher) for 72 h to select for transfected cells. Clones were isolated using a FACS Melody (BD Biosciences) cell sorter into 96-well plates. Individual clones with MCM8 and MCM9 knockout were confirmed using NGS sequencing (Genewiz).

Immunofluorescence

Adherent cells were washed in PBS (2 times), fixed in 4% paraformaldehyde in PBS for 10 min, and permeabilized with 0.1% Triton X-100 in PBS (PBST) for 15 min. Cells were blocked overnight with 5% BSA in PBST at 4 °C and then incubated with 1:50 RAD51 primary antibody (sc-8349, Santa Cruz or ab63801, Abcam) or 1:50 BRCA1 primary antibody (sc-6954, Santa Cruz) in 2.5% BSA in PBST for 1 h at 37 °C. Cells were washed three times in PBST and incubated with 1:50 dilution of the appropriate fluorescent secondary antibody followed by wash with PBST (three times). Cells were mounted in DAPI mountant (Prolong Gold, Thermo Fisher) and sealed with clear polish, and imaged under a FV-1000 epifluorescence or FV-3000 confocal laser scanning microscope (Olympus Corp). Images were processed with vendor included Fluoview (v.4.2 b) or CellSens (v2.2) software. For suspension of EBV transfected lymphocytes, cells were immunostained similar to adherent cells but were harvested by centrifugation after MMC treatment, and immunostaining was performed in suspension. To mount the cells, they were resuspended in 1 µl of mountant and placed on a coverslip, which was then picked up using a microscopic slide, and sealed with clear polish. RAD51 foci from epifluorescence images were automatically counted from individually gated cells using identical thresholds that eliminated background noise using Image J (84). Foci per cell are presented in a dot plot, averaged, and the standard error reported.

Subcellular fractionation

HEK293T cells transfected with EGFP constructs containing MCM9 truncations/mutations were cultured in 6-well plates and harvested. Fractionation into nuclear and cytoplasmic portions was carried out according to manufacturer's directions using a Nuclear/Cytosol Fractionation Kit (K266, BioVision). Equal volumes of protein were loaded onto a 12% acrylamide gel and transferred to PVDF membranes.

Membranes were probed with the following primary antibodies: mouse anti-GFP (Invitrogen, MA5-15256), rabbit anti-Lamin B1 (Proteintech, 12987-1-AP), mouse anti-αTubulin (Proteintech, 66031-1-Ig), and/or mouse anti-GAPDH (Developmental Studies Hybridoma Bank, DSHB-hGAPDH-2G7). Membranes were incubated with goat anti-mouse (Novex, A16072) or goat anti-rabbit (Novex, A16096) HRP-conjugated secondary antibodies and visualized using luminol reagent (Santa Cruz Biotechnology, sc-2048). For fluorescent detection, membranes were incubated with α-rabbit IgG-Alexa488 or α-mouse IgG-Alexa647 conjugates (Thermo Fisher). Membranes were scanned using the LAS 4000 imager (Cytiva). The nuclear-to-cytoplasmic (N/C) ratio was calculated by subtracting the background from the MCM9-GFP construct bands using ImageQuant v.7.0 (Cytiva), normalizing to the average N/C ratio of the controls, and then dividing the resulting nuclear and cytoplasmic fractions. The standard error is the result of three independent experiments, and the *p*-values are calculated using a standard two-tailed *t*-test.

Affinity pull-down

GST-tagged RAD51 (4 µM) was added to glutathione agarose (UBPBio) on ice for 30 min before spinning down and removing the supernatant. Then, an equal molar amount of purified MCM9 (643–900) was added and incubated for 30 min, mixing every 10 min. Samples were spun down, and supernatant was reserved as the flow-through. The GST-agarose was washed with an equal volume of GST-binding buffer (20 mM HEPES [pH 7.5], 75 mM NaCl, 0.1 mM EDTA, 1 mM BME, and 10% glycerol) and centrifuged for 60 s at 8000g at least seven times. Proteins were eluted with an equal amount of GST elution buffer (20 mM HEPES [pH 8.0], 300 mM NaCl, 1 mM EDTA, 10 mM BME, and 10% glycerol, and 10 mM reduced glutathione). Eluted samples were separated using 10% SDS-PAGE gels and stained with Coomassie.

Yeast two-hybrid assay

To generate the yeast two-hybrid plasmids, full-length (1–1143) or C-term (620–1143) was inserted into pGBKT7 (Clontech) using *SmaI*/*SalI* restrictions sites. The BRCv (687FR→AA) mutation was created by Quikchange mutagenesis (Agilent Genomics) using Kapa DNA polymerase (Kapa Biosystems) and screened with novel silent restriction sites. RAD51 was PCR amplified from pGAT3-RAD51 (81) with primers that included *MfeI* and *XhoI* sites and then ligated into pGADT7 (Clontech) digested with *EcoRI*/*XhoI*. The yeast strain SFY526 (MATa, ura3-52, his3-200, ade2-101, lys2-801, trp1-901, leu2-3, 112, canr, gal4-542, gal80–538, URA::GAL1UAS-GAL1TATA-lacZ) was transformed with the appropriate plasmids (see figure legends) according to the manufacturer's instructions using the lithium acetate procedure (Clontech Matchmaker 2 manual). Liquid cultures were grown overnight in standard dropout (SD) media lacking tryptophan and leucine. The cells were restreaked onto SD/-Trp/-Leu and incubated at 30 °C for 2 to 3 days before

performing a colony-lift β-galactosidase assay (X-gal, Sigma-Aldrich) according to the Yeast Protocols Handbook (PT3024-1, Clontech).

Data availability

All data are contained within the article.

Conflicts of interest—The authors declare that they have no conflicts of interest with the contents of this article.

Abbreviations—The abbreviations used are: BER, base excision repair; BME, β-mercaptoethanol; BRC, breast cancer; BRCA1, breast cancer type 1 susceptibility protein; BRCA2, breast cancer type 2 susceptibility protein; BRCv, BRC variant motif; BSA, bovine serum albumin; CD, circular dichroism; Cis-Pt, cisplatin; cNLS, classic NLS; CTE, C-terminal extension; DAPI, 4′,6-diamindino-2-phenylindole; DMEM, Dulbecco's modified Eagle's medium; DSB, double-strand break; dsDNA, double-stranded DNA; EBV, Epstein–Barr virus; EDTA, ethylenediaminetetraacetic acid; FA, Fanconi anemia; FBS, fetal bovine serum; GAPDH, glyceraldehyde-3-phosphate dehydrogenase; GFP, green fluorescent protein; GST, glutathione S-transferase; HEK, human embryonic kidney (cells); HEPES, hydroxyethyl piperazineethanesulfonic acid; HRP, horseradish peroxidase; HR, homologous recombination; ICL, interstrand cross-link; IPTG, isopropyl β-D-thiogalactopyranosidase; KD, knockdown; KO, knockout; LPEI, linear polyethyleneimine; MCM, minichromosomal maintenance; MMC, mitomycin-C; MMR, mismatch repair; MRN, Mre11/ Rad50/ Nbs1 complex; NER, nucleotide excision repair; NLS, nuclear localization signal; NTD, N-terminal domain; OD, ocular density; PARP, poly(ADP-ribose) polymerase; PBS, phosphate-buffered saline; pCHK1, phosphorylated checkpoint kinase 1; PMSF, phenylmethylsulfonyl fluoride; pNLS, putative NLS; PVDF, polyvinylidene difluoride; RPA, replication protein A; RPMI, Roswell Park Memorial Institute media; SDS-PAGE, sodium dodecyl sulfate–polyacrylamide gel electrophoresis; ssDNA, single-stranded DNA; TEV, tobacco etch virus; TLS, translesion synthesis; U2OS, human bone osteosarcoma epithelial cells; WT, wild type; XRCC, X-ray repair cross complementing; Y2H, yeast two-hybrid.

References

1. Wright, W. D., Shah, S. S., and Heyer, W. D. (2018) Homologous recombination and the repair of DNA double-strand breaks. *J. Biol. Chem.* **293**, 10524–10535
2. Quinet, A., Lemacon, D., and Vindigni, A. (2017) Replication fork reversal: Players and guardians. *Mol. Cell* **68**, 830–833
3. Hunter, N. (2015) Meiotic recombination: The essence of heredity. *Cold Spring Harb. Perspect. Biol.* **7**, a016618
4. Crickard, J. B., and Greene, E. C. (2018) The biochemistry of early meiotic recombination intermediates. *Cell Cycle* **17**, 2520–2530
5. Huselid, E., and Bunting, S. F. (2020) The regulation of homologous recombination by helicases. *Genes (Basel)* **11**, 498
6. Griffin, W. C., and Trakselis, M. A. (2019) The MCM8/9 complex: A recent recruit to the roster of helicases involved in genome maintenance. *DNA Repair (Amst.)* **76**, 1–10
7. Gambus, A., and Blow, J. J. (2013) Mcm8 and Mcm9 form a dimeric complex in *Xenopus laevis* egg extract that is not essential for DNA replication initiation. *Cell Cycle* **12**, 1225–1232
8. Dungrawala, H., Rose, K. L., Bhat, K. P., Mohni, K. N., Glick, G. G., Couch, F. B., and Cortez, D. (2015) The replication checkpoint prevents two types of fork collapse without regulating replisome stability. *Mol. Cell* **59**, 998–1010
9. Natsume, T., Nishimura, K., Minocherhomji, S., Bhowmick, R., Hickson, I. D., and Kanemaki, M. T. (2017) Acute inactivation of the replicative helicase in human cells triggers MCM8-9-dependent DNA synthesis. *Genes Dev.* **31**, 816–829
10. Lee, K. Y., Im, J. S., Shibata, E., Park, J., Handa, N., Kowalczykowski, S. C., and Dutta, A. (2015) MCM8-9 complex promotes resection of double-strand break ends by MRE11-RAD50-NBS1 complex. *Nat. Commun.* **6**, 7744
11. Nishimura, K., Ishiai, M., Horikawa, K., Fukagawa, T., Takata, M., Takisawa, H., and Kanemaki, M. T. (2012) Mcm8 and Mcm9 form a complex that functions in homologous recombination repair induced by DNA interstrand crosslinks. *Mol. Cell* **47**, 511–522
12. Park, J., Long, D. T., Lee, K. Y., Abbas, T., Shibata, E., Negishi, M., Luo, Y., Schimenti, J. C., Gambus, A., Walter, J. C., and Dutta, A. (2013) The MCM8-MCM9 complex promotes RAD51 recruitment at DNA damage sites to facilitate homologous recombination. *Mol. Cell. Biol.* **33**, 1632–1644
13. Hustedt, N., Saito, Y., Zimmermann, M., Alvarez-Quilon, A., Setiaputra, D., Adam, S., McEwan, A., Yuan, J. Y., Olivieri, M., Zhao, Y., Kanemaki, M. T., Jurisicova, A., and Durocher, D. (2019) Control of homologous recombination by the HROB-MCM8-MCM9 pathway. *Genes Dev.* **33**, 1397–1415
14. Lutzmann, M., Grey, C., Traver, S., Ganier, O., Maya-Mendoza, A., Ranisavljevic, N., Bernex, F., Nishiyama, A., Montel, N., Gavois, E., Forichon, L., de Massy, B., and Mechali, M. (2012) MCM8- and MCM9-deficient mice reveal gametogenesis defects and genome instability due to impaired homologous recombination. *Mol. Cell* **47**, 523–534
15. Hartford, S. A., Luo, Y., Southard, T. L., Min, I. M., Lis, J. T., and Schimenti, J. C. (2011) Minichromosome maintenance helicase paralog MCM9 is dispensable for DNA replication but functions in germ-line stem cells and tumor suppression. *Proc. Natl. Acad. Sci. U. S. A.* **108**, 17702–17707
16. Bhat, K. P., and Cortez, D. (2018) RPA and RAD51: Fork reversal, fork protection, and genome stability. *Nat. Struct. Mol. Biol.* **25**, 446–453
17. AlAsiri, S., Basit, S., Wood-Trageser, M. A., Yatsenko, S. A., Jeffries, E. P., Surti, U., Ketterer, D. M., Afzal, S., Ramzan, K., Faiyaz-Ul Haque, M., Jiang, H., Trakselis, M. A., and Rajkovic, A. (2015) Exome sequencing reveals MCM8 mutation underlies ovarian failure and chromosomal instability. *J. Clin. Invest.* **125**, 258–262
18. Wood-Trageser, M. A., Gurbuz, F., Yatsenko, S. A., Jeffries, E. P., Kotan, L. D., Surti, U., Ketterer, D. M., Matic, J., Chipkin, J., Jiang, H., Trakselis, M. A., Topaloglu, A. K., and Rajkovic, A. (2014) MCM9 mutations are associated with ovarian failure, short stature, and chromosomal instability. *Am. J. Hum. Genet.* **95**, 754–762

ASBMB

19. Desai, S., Wood-Trageser, M., Matic, J., Chipkin, J., Jiang, H., Bachelot, A., Dulon, J., Sala, C., Barbieri, C., Cocca, M., Toniolo, D., Touraine, P., Witchel, S., and Rajkovic, A. (2017) MCM8 and MCM9 nucleotide variants in women with primary ovarian insufficiency. *J. Clin. Endocrinol. Metab.* **102**, 576–582

20. Goldberg, Y., Halpern, N., Hubert, A., Adler, S. N., Cohen, S., Plesser-Duvdevani, M., Pappo, O., Shaag, A., and Meiner, V. (2015) Mutated MCM9 is associated with predisposition to hereditary mixed polyposis and colorectal cancer in addition to primary ovarian failure. *Cancer Genet.* **208**, 621–624

21. Giampietro, P. F., Adler-Brecher, B., Verlander, P. C., Pavlakis, S. G., Davis, J. G., and Auerbach, A. D. (1993) The need for more accurate and timely diagnosis in Fanconi anemia: A report from the International Fanconi Anemia Registry. *Pediatrics* **91**, 1116–1120

22. Alter, B. P., Frissora, C. L., Halperin, D. S., Freedman, M. H., Chitkara, U., Alvarez, E., Lynch, L., Adler-Brecher, B., and Auerbach, A. D. (1991) Fanconi's anaemia and pregnancy. *Br. J. Haematol.* **77**, 410–418

23. Poulogiannis, G., Frayling, I. M., and Arends, M. J. (2010) DNA mismatch repair deficiency in sporadic colorectal cancer and Lynch syndrome. *Histopathology* **56**, 167–179

24. Traver, S., Coulombe, P., Peiffer, I., Hutchins, J. R., Kitzmann, M., Latreille, D., and Mechali, M. (2015) MCM9 is required for mammalian DNA mismatch repair. *Mol. Cell* **59**, 831–839

25. Tham, K. C., Kanaar, R., and Lebbink, J. H. G. (2016) Mismatch repair and homeologous recombination. *DNA Repair (Amst.)* **38**, 75–83

26. Spies, M., and Fishel, R. (2015) Mismatch repair during homologous and homeologous recombination. *Cold Spring Harb. Perspect. Biol.* **7**, a022657

27. Kato, N., Kawasoe, Y., Williams, H., Coates, E., Roy, U., Shi, Y., Beese, L. S., Scharer, O. D., Yan, H., Gottesman, M. E., Takahashi, T. S., and Gautier, J. (2017) Sensing and processing of DNA interstrand crosslinks by the mismatch repair pathway. *Cell Rep.* **21**, 1375–1385

28. Yang, W. (2008) Structure and mechanism for DNA lesion recognition. *Cell Res.* **18**, 184–197

29. Kim, J. H., Dhanasekaran, S. M., Mehra, R., Tomlins, S. A., Gu, W., Yu, J., Kumar-Sinha, C., Cao, X., Dash, A., Wang, L., Ghosh, D., Shedden, K., Montie, J. E., Rubin, M. A., Pienta, K. J., *et al.* (2007) Integrative analysis of genomic aberrations associated with prostate cancer progression. *Cancer Res.* **67**, 8229–8239

30. Sung, C. O., Kim, S. C., Karnan, S., Karube, K., Shin, H. J., Nam, D. H., Suh, Y. L., Kim, S. H., Kim, J. Y., Kim, S. J., Kim, W. S., Seto, M., and Ko, Y. H. (2011) Genomic profiling combined with gene expression profiling in primary central nervous system lymphoma. *Blood* **117**, 1291–1300

31. He, D. M., Ren, B. G., Liu, S., Tan, L. Z., Cieply, K., Tseng, G., Yu, Y. P., and Luo, J. H. (2017) Oncogenic activity of amplified miniature chromosome maintenance 8 in human malignancies. *Oncogene* **36**, 3629–3639

32. Morii, I., Iwabuchi, Y., Mori, S., Suekuni, M., Natsume, T., Yoshida, K., Sugimoto, N., Kanemaki, M. T., and Fujita, M. (2019) Inhibiting the MCM8-9 complex selectively sensitizes cancer cells to cisplatin and olaparib. *Cancer Sci.* **110**, 1044–1053

33. Jeffries, E. P., Denq, W. I., Bartko, J. C., and Trakselis, M. A. (2013) Identification, quantification, and evolutionary analysis of a novel isoform of MCM9. *Gene* **519**, 41–49

34. Islam, M. N., Paquet, N., Fox, D., 3rd, Dray, E., Zheng, X. F., Klein, H., Sung, P., and Wang, W. (2012) A variant of the breast cancer type 2 susceptibility protein (BRC) repeat is essential for the RECQL5 helicase to interact with RAD51 recombinase for genome stabilization. *J. Biol. Chem.* **287**, 23808–23818

35. Chemes, L. B., Alonso, L. G., Noval, M. G., and de Prat-Gay, G. (2012) Circular dichroism techniques for the analysis of intrinsically disordered proteins and domains. *Methods Mol. Biol.* **895**, 387–404

36. Shivji, M. K., Mukund, S. R., Rajendra, E., Chen, S., Short, J. M., Savill, J., Klenerman, D., and Venkitaraman, A. R. (2009) The BRC repeats of human BRCA2 differentially regulate RAD51 binding on single- versus double-stranded DNA to stimulate strand exchange. *Proc. Natl. Acad. Sci. U. S. A.* **106**, 13254–13259

37. Pichierri, P., Averbeck, D., and Rosselli, F. (2002) DNA cross-link-dependent RAD50/MRE11/NBS1 subnuclear assembly requires the Fanconi anemia C protein. *Hum. Mol. Genet.* **11**, 2531–2546

38. Bunting, S. F., Callen, E., Kozak, M. L., Kim, J. M., Wong, N., Lopez-Contreras, A. J., Ludwig, T., Baer, R., Faryabi, R. B., Malhowski, A., Chen, H. T., Fernandez-Capetillo, O., D'Andrea, A., and Nussenzweig, A. (2012) BRCA1 functions independently of homologous recombination in DNA interstrand crosslink repair. *Mol. Cell* **46**, 125–135

39. Schlacher, K., Wu, H., and Jasin, M. (2012) A distinct replication fork protection pathway connects Fanconi anemia tumor suppressors to RAD51-BRCA1/2. *Cancer Cell* **22**, 106–116

40. Rickman, K., and Smogorzewska, A. (2019) Advances in understanding DNA processing and protection at stalled replication forks. *J. Cell Biol.* **218**, 1096–1107

41. Garcia-Higuera, I., Taniguchi, T., Ganesan, S., Meyn, M. S., Timmers, C., Hejna, J., Grompe, M., and D'Andrea, A. D. (2001) Interaction of the Fanconi anemia proteins and BRCA1 in a common pathway. *Mol. Cell* **7**, 249–262

42. Liu, Y., Richards, T. A., and Aves, S. J. (2009) Ancient diversification of eukaryotic MCM DNA replication proteins. *BMC. Evol. Biol.* **9**, 60

43. Allen, G. C., Jr., and Kornberg, A. (1991) The priB gene encoding the primosomal replication n protein of *Escherichia coli. J. Biol. Chem.* **266**, 11610–11613

44. Pryor, J. M., Dieckman, L. M., Boehm, E. M., and Washington, M. T. (2014) Eukaryotic Y-family polymerases: A biochemical and structural perspective. In: Murakami, K. S., Trakselis, M. A., eds. *Nucleic Acids and Molecular Biology*, Springer-Verlag, Berlin: 85–108

45. Parker, M. W., Bell, M., Mir, M., Kao, J. A., Darzacq, X., Botchan, M. R., and Berger, J. M. (2019) A new class of disordered elements controls DNA replication through initiator self-assembly. *Elife* **8**, e48562

46. Kim, Y., Furman, C. M., Manhart, C. M., Alani, E., and Finkelstein, I. J. (2019) Intrinsically disordered regions regulate both catalytic and non-catalytic activities of the MutL mismatch repair complex. *Nucleic Acids Res.* **47**, 1823–1835

47. Iakoucheva, L. M., Kimzey, A. L., Masselon, C. D., Bruce, J. E., Garner, E. C., Brown, C. J., Dunker, A. K., Smith, R. D., and Ackerman, E. J. (2001) Identification of intrinsic order and disorder in the DNA repair protein XPA. *Protein Sci.* **10**, 560–571

48. Zou, Y., Liu, Y. Y., Wu, X. M., and Shell, S. M. (2006) Functions of human replication protein A (RPA): From DNA replication to DNA damage and stress responses. *J. Cell. Physiol.* **208**, 267–273

49. Laptenko, O., Tong, D. R., Manfredi, J., and Prives, C. (2016) The tail that wags the dog: How the disordered C-terminal domain controls the transcriptional activities of the p53 tumor-suppressor protein. *Trends Biochem. Sci.* **41**, 1022–1034

50. Kalderon, D., Richardson, W. D., Markham, A. F., and Smith, A. E. (1984) Sequence requirements for nuclear location of simian virus 40 large-T antigen. *Nature* **311**, 33–38

51. Dingwall, C., and Laskey, R. A. (1991) Nuclear targeting sequences–a consensus? *Trends Biochem. Sci.* **16**, 478–481

52. Robbins, J., Dilworth, S. M., Laskey, R. A., and Dingwall, C. (1991) Two interdependent basic domains in nucleoplasmin nuclear targeting sequence: Identification of a class of bipartite nuclear targeting sequence. *Cell* **64**, 615–623

53. Xiao, Z., Latek, R., and Lodish, H. F. (2003) An extended bipartite nuclear localization signal in Smad4 is required for its nuclear import and transcriptional activity. *Oncogene* **22**, 1057–1069

54. Kim, K. H., Kanbe, T., Akashi, T., Mizuguchi, I., and Kikuchi, A. (2002) Identification of a single nuclear localization signal in the C-terminal domain of an *Aspergillus* DNA topoisomerase II. *Mol. Genet. Genomics* **268**, 287–297

55. Masson, M., Niedergang, C., Schreiber, V., Muller, S., Menissier-de Murcia, J., and de Murcia, G. (1998) XRCC1 is specifically associated with poly(ADP-ribose) polymerase and negatively regulates its activity following DNA damage. *Mol. Cell. Biol.* **18**, 3563–3571

56. Kirby, T. W., Gassman, N. R., Smith, C. E., Pedersen, L. C., Gabel, S. A., Sobhany, M., Wilson, S. H., and London, R. E. (2015) Nuclear localization of the DNA repair scaffold XRCC1: Uncovering the functional role of a bipartite NLS. *Sci. Rep.* **5**, 13405

57. Moore, S. P., Rinckel, L. A., and Garfinkel, D. J. (1998) A Ty1 integrase nuclear localization signal required for retrotransposition. *Mol. Cell. Biol.* **18**, 1105–1114

58. Lange, A., McLane, L. M., Mills, R. E., Devine, S. E., and Corbett, A. H. (2010) Expanding the definition of the classical bipartite nuclear localization signal. *Traffic* **11**, 311–323

59. Fontes, M. R., Teh, T., and Kobe, B. (2000) Structural basis of recognition of monopartite and bipartite nuclear localization sequences by mammalian importin-alpha. *J. Mol. Biol.* **297**, 1183–1194

60. Conti, E., and Kuriyan, J. (2000) Crystallographic analysis of the specific yet versatile recognition of distinct nuclear localization signals by karyopherin alpha. *Structure* **8**, 329–338

61. Gorlich, D., Kostka, S., Kraft, R., Dingwall, C., Laskey, R. A., Hartmann, E., and Prehn, S. (1995) Two different subunits of importin cooperate to recognize nuclear localization signals and bind them to the nuclear envelope. *Curr. Biol.* **5**, 383–392

62. Nash, R. A., Caldecott, K. W., Barnes, D. E., and Lindahl, T. (1997) XRCC1 protein interacts with one of two distinct forms of DNA ligase III. *Biochemistry* **36**, 5207–5211

63. Deans, A. J., and West, S. C. (2011) DNA interstrand crosslink repair and cancer. *Nat. Rev. Cancer* **11**, 467–480

64. Muniandy, P. A., Liu, J., Majumdar, A., Liu, S. T., and Seidman, M. M. (2010) DNA interstrand crosslink repair in mammalian cells: Step by step. *Crit. Rev. Biochem. Mol. Biol.* **45**, 23–49

65. Eastman, A. (1986) Reevaluation of interaction of cis-dichloro(ethylenediamine)platinum(II) with DNA. *Biochemistry* **25**, 3912–3915

66. Bizanek, R., McGuinness, B. F., Nakanishi, K., and Tomasz, M. (1992) Isolation and structure of an intrastrand cross-link adduct of mitomycin C and DNA. *Biochemistry* **31**, 3084–3091

67. Teng, S. P., Woodson, S. A., and Crothers, D. M. (1989) DNA sequence specificity of mitomycin cross-linking. *Biochemistry* **28**, 3901–3907

68. Huang, H., Zhu, L., Reid, B. R., Drobny, G. P., and Hopkins, P. B. (1995) Solution structure of a cisplatin-induced DNA interstrand cross-link. *Science* **270**, 1842–1845

69. Rink, S. M., Lipman, R., Alley, S. C., Hopkins, P. B., and Tomasz, M. (1996) Bending of DNA by the mitomycin C-induced, GpG intrastrand cross-link. *Chem. Res. Toxicol.* **9**, 382–389

70. Furuta, T., Ueda, T., Aune, G., Sarasin, A., Kraemer, K. H., and Pommier, Y. (2002) Transcription-coupled nucleotide excision repair as a determinant of cisplatin sensitivity of human cells. *Cancer Res.* **62**, 4899–4902

71. Welsh, C., Day, R., McGurk, C., Masters, J. R. W., Wood, R. D., and Koberle, B. (2004) Reduced levels of XPA, ERCC1 and XPF DNA repair proteins in testis tumor cell lines. *Int. J. Cancer* **110**, 352–361

72. Fink, D., Nebel, S., Aebi, S., Zheng, H., Cenni, B., Nehme, A., Christen, R. D., and Howell, S. B. (1996) The role of DNA mismatch repair in platinum drug resistance. *Cancer Res.* **56**, 4881–4886

73. Zhao, J. H., Jain, A., Iyer, R. R., Modrich, P. L., and Vasquez, K. M. (2009) Mismatch repair and nucleotide excision repair proteins cooperate in the recognition of DNA interstrand crosslinks. *Nucleic Acids Res.* **37**, 4420–4429

74. Lee, Y. J., Park, S. J., Ciccone, S. L. M., Kim, C. R., and Lee, S. H. (2006) An *in vivo* analysis of MMC-induced DNA damage and its repair. *Carcinogenesis* **27**, 446–453

75. Kyte, J., and Doolittle, R. F. (1982) A simple method for displaying the hydropathic character of a protein. *J. Mol. Biol.* **157**, 105–132

76. Ward, J. J., Sodhi, J. S., McGuffin, L. J., Buxton, B. F., and Jones, D. T. (2004) Prediction and functional analysis of native disorder in proteins from the three kingdoms of life. *J. Mol. Biol.* **337**, 635–645

77. Jones, D. T. (1999) Protein secondary structure prediction based on position-specific scoring matrices. *J. Mol. Biol.* **292**, 195–202

78. Kosugi, S., Hasebe, M., Tomita, M., and Yanagawa, H. (2009) Systematic identification of cell cycle-dependent yeast nucleocytoplasmic shuttling proteins by prediction of composite motifs. *Proc. Natl. Acad. Sci. U. S. A.* **106**, 10171–10176

79. Waterhouse, A., Bertoni, M., Bienert, S., Studer, G., Tauriello, G., Gumienny, R., Heer, F. T., de Beer, T. A. P., Rempfer, C., Bordoli, L., Lepore, R., and Schwede, T. (2018) SWISS-MODEL: Homology modelling of protein structures and complexes. *Nucleic Acids Res.* **46**, W296–W303

80. Benkert, P., Kunzli, M., and Schwede, T. (2009) QMEAN server for protein model quality estimation. *Nucleic Acids Res.* **37**, W510–W514

81. Davies, O. R., and Pellegrini, L. (2007) Interaction with the BRCA2 C terminus protects RAD51-DNA filaments from disassembly by BRC repeats. *Nat. Struct. Mol. Biol.* **14**, 475–483

82. Micsonai, A., Wien, F., Bulyaki, E., Kun, J., Moussong, E., Lee, Y. H., Goto, Y., Refregiers, M., and Kardos, J. (2018) BeStSel: A web server for accurate protein secondary structure prediction and fold recognition from the circular dichroism spectra. *Nucleic Acids Res.* **46**, W315–W322

83. Micsonai, A., Wien, F., Kernya, L., Lee, Y. H., Goto, Y., Refregiers, M., and Kardos, J. (2015) Accurate secondary structure prediction and fold recognition for circular dichroism spectroscopy. *Proc. Natl. Acad. Sci. U. S. A.* **112**, E3095–E3103

84. Rasband, W. S. (2015) *(1997-2016) ImageJ*, U. S. National Institutes of Health, Bethesda, MD